

---

# Synthesis and Processing of Nanomaterials

## Contents

Introduction .....	748
Vapor, Spray, and Plasma Processes .....	749
Electrodeposition .....	759
Fabrication of Bulk Nanocrystalline Materials by Severe Plastic Deformation Processes .....	761
References .....	765

---

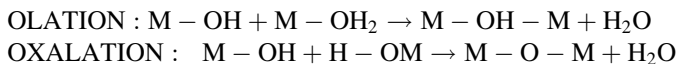
## Abstract

Nanoparticles and nanoparticle aggregates are produced as colloids and related nanocrystals by sol–gel and wet chemical synthesis as well as a variety of vapor, spray, and plasma processes, including flames. Vapor-phase material can be condensed or deposited on variously heated or cooled substrates, even crystalline substrates where films, islands, and quantum dots can be grown. The role of catalysts in promoting reactions is described. Sputter deposition and other physical vapor deposition (PVD) processes are discussed, including arc evaporation. Chemical vapor deposition (CVD), including reaction product production and collection, is presented. Molecular beam epitaxy (MBE) and atomic layer deposition are described. Collected nanopowders can be statically or dynamically consolidated to form bulk billets. Mechanical alloying and mechanochemical synthesis of nanomaterials are discussed along with electrodeposition, friction-stir processing (FSP), and equal-channel angular processing (ECAP) or extrusion as these apply to severe plastic deformation (SPD) processes to produce nanocrystalline bulk solids.

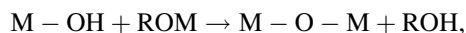
## Introduction

Because there are so many types or classifications of nanomaterials and structures, there are correspondingly a great variety of synthesis and processing routes to achieve them, especially in commercial quantities, some of which, such as black carbons, require tens of millions of tons globally on an annual basis. Thermodynamic modifications of pyrolysis processes (organic decomposition in the absence of oxygen) for the synthesis of black carbons are also used to produce varieties of graphites as well as carbon nanotubes. The production of nanometals such as gold and silver as described in Part XI, chapter “► [3D Printing: Printed Electronics](#),” characterizes chemical reaction routes involving stabilization and reducing agents (Zhao et al. 2013). Similar chemical processes involve the sol–gel process, a wet chemical technique for producing colloidal particles (<30 nm) or particle networks (Brinker and Scherer 1990). Nanoparticles are also produced by a variety of physical processes involving spraying or deposition techniques, while bulk nanocrystalline materials generally require mechanical or deformation processing (Tjong and Chen 2004).

The so-called liquid synthesis routes such as *sol–gel processing* or *wet chemical synthesis* are especially conducive to producing metal oxide or ceramic nanoparticles such as those illustrated in ► [Fig. 3 in chapter “Classifications and Structures of Nanomaterials.”](#) The sol–gel process offers a degree of control over composition and structure, even at the molecular level, through the production of a colloidal suspension (or sol) which is converted to a viscous gel or solid nanoparticulate. In this process, reactive metal precursors are initially hydrolyzed followed by condensation and polymerization reactions. Two mononuclear complexes of a metal, M, each comprising only one metal, M, can react to form a polynuclear complex consisting of two metal atoms. Condensation occurs via the so-called olation and oxalation reactions as follows:



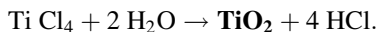
or



where R is an alkyl group,  $\text{C}_n\text{H}_{2n+1}$ . Under acidic conditions, 3D solid-phase networks form consisting of extended linear  $\text{M} - \text{O} - \text{M}$  chain molecules.

Wet chemical processes, including solid nanoparticle precipitation from supersaturated solution, homogeneous liquid-phase chemical reduction, or ultrasonic decomposition of chemical precursors, are particularly attractive because of their simplicity, versatility, and low cost. For example, titania ( $\text{TiO}_2$ ) nanoparticle

production as illustrated in ► [Fig. 3b of chapter “Classifications and Structures of Nanomaterials”](#) by hydrolysis of  $\text{TiCl}_4$  at low temperatures is expressed as



It is probably notable to indicate that nanoparticle synthesis of gold, silver, and copper in particular has been observed and studied in a number of biomimetic or “green” synthesis regimes including bacteria (Anastas and Warner 2000), fungi (Ahmad et al. 2003), and plants, where plant components uptake metal ions from the soil and produce small, colloidal, or neutral nanogold, copper, or silver crystals or polycrystal forms (MarChiol 2012; Das and Marsili 2010). In these processes the reduced, neutral metal nanoparticles can be recovered by simple combustion of the organic matrix. These regimes often produce very small crystalline, nanometal particles,  $\sim 5$  nm in diameter, in contrast to other processes or synthesis routes where precipitation or reduction can produce colloidal ( $\leq 30$  nm diameter) or larger nanoparticles ( $\sim 50$ – $100$  nm).

---

## Vapor, Spray, and Plasma Processes

Over the past two decades, various process technologies have been developed for producing a variety of nanomaterials or nanostructure forms: particles, films, or bulk-related (3D) nanomaterials by vapor condensation and especially rapid solidification, from atomized (vapor), aerosol, or liquid jets and sprays (Tjong and Chen 2004). Figures 1–7 illustrate a variety of these techniques, several of which are conceptually similar.

Figure 1 illustrates a variety of plasma synthesis techniques for producing nanoparticles. Figure 1a shows a flame which may conceptually be considered a partial plasma. In combustion flames such as propane ( $\text{C}_2\text{H}_8$ ) or natural gas (methane,  $\text{CH}_4$ ), variations in oxygen or air flow can alter the production of carbon nanoparticles, including soots, fullerenes, or carbon nanotubes. These can be collected electrostatically. Figure 2 illustrates multiwall carbon nanotube–multiwall (or multiconcentric) fullerene nanoparticle aggregates collected above a propane and methane (natural gas) flame, respectively, and observed in the TEM. Precursor materials, mixtures, or premixed gases can also be used to synthesize nanoparticles, for example, titania can be synthesized in a flame from premixed  $\text{TiCl}_4 + \text{CH}_4 + \text{O}_2$ . Using an electrostatic plate collection system not only collects  $\text{TiO}_2$  product, but the product is less aggregated and primary particles are smaller, nanoscale particles.

High-temperature plasma processes can use DC, AC, or RF power sources for nanopowder production using either liquid or solid powder precursors. Figure 1b shows two plasma synthesis arrangements. In the axial feed precursor on the left, a sheath gas draws the precursor into the system. Feeding the precursor into the plasma (flame) as illustrated in the right schematic in Fig. 1b is used for powder precursors. For RF plasmas, the nozzle design becomes crucial. Rapid cooling of

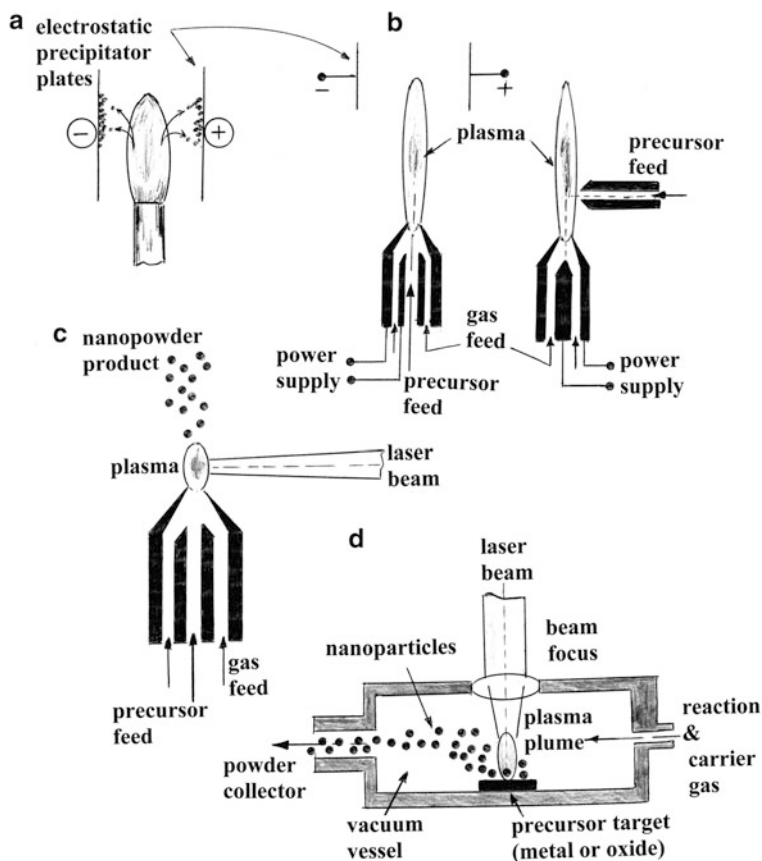
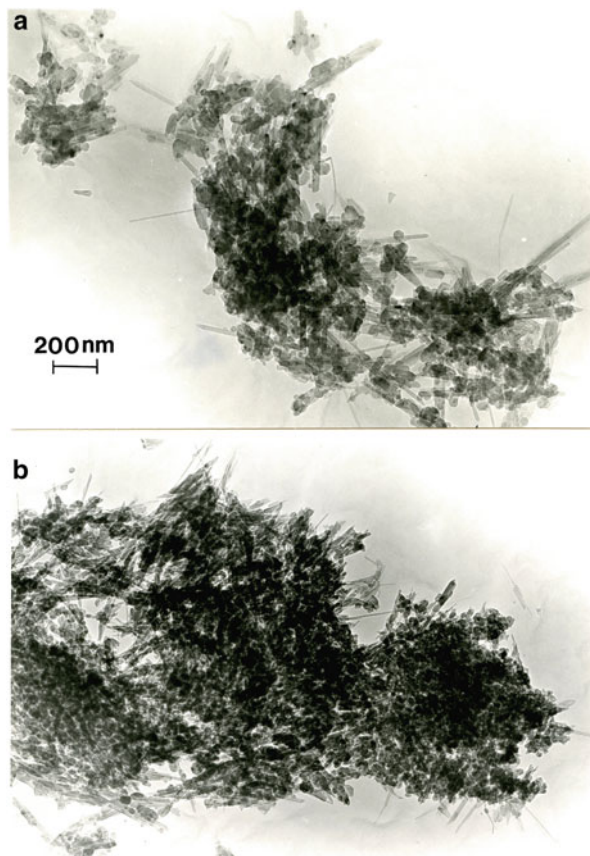


**Fig. 1** Schematic views of plasma processes for nanoparticle synthesis. (a) Simple combustion flame with electrostatic collection plates. (b) Two basic and most plasma burners operating at atmospheric pressure using DC or AC power. Plasma burns between two coaxial electrodes, which are cooled by gas flow as well. (c) Laser-driven plasma system. (d) Laser ablation process. Reaction product is carried to cold surface or electrostatic collectors

the gas following reaction in the plasma is also important in controlling the nanoparticle size and size distribution as well as the degree of aggregation. In this respect, it is possible to project the plasma-generated nanoparticle stream onto a rotating, liquid nitrogen drum instead of collecting the product stream on the electrostatic precipitator plates.

In Fig. 1c the plasma is created by a focused laser beam. Reactant concentration is normally high since the focal point is just above the orifice, and this situation often creates agglomerated nanoparticles. Figure 1d utilizes laser ablation where the beam is focused onto a metal, alloy, or metal oxide target which is vaporized instantaneously, preserving the stoichiometry of the target. The supersonic, ionized vapor jet or plume of evaporated material in Fig. 1d can reach temperatures

**Fig. 2** Flame-produced multiwall carbon nanotube–fullerene aggregates observed in the TEM. (a) Propane flame. (b) Methane (natural gas) flame. Natural gas is 96 % methane



exceeding 3,800 K. Particle growth in the cooling, supersaturated plume is limited by system gas pressure. Increasing the supersaturation increases the number of nuclei and correspondingly decreases nanoparticle size in the powder product which can be collected electrostatically or on a cooled, rotating drum.

Cooled, rotating drum collectors originated in the 1960s when amorphous or glassy metal (or alloy) products were formed by supercooling on a liquid nitrogen cooled, rotating drum as illustrated schematically in Fig. 3a. In this process, liquid metals or alloys are projected onto the cooled drum, often referred to as a casting wheel. This process produced thin, even controlled thicknesses of amorphous ribbon which was rapidly stripped from the drum, often 3–5 cm in width and <100  $\mu\text{m}$  thick, corresponding to cooling rates ranging from  $\sim 10^6$   $^\circ\text{C}/\text{s}$  to  $10^7$   $^\circ\text{C}/\text{s}$ . These amorphous strips could be flash annealed to produce a brittle, nanocrystalline product which could be easily crushed to the nanograin size (Lu 1996). This process (Fig. 3a) was modified slightly as shown schematically in Fig. 3b to produce an aerosol precursor by mixing Ar gas with the jetting liquid. This produced a nanoparticle product which was scrapped from the cold drum.

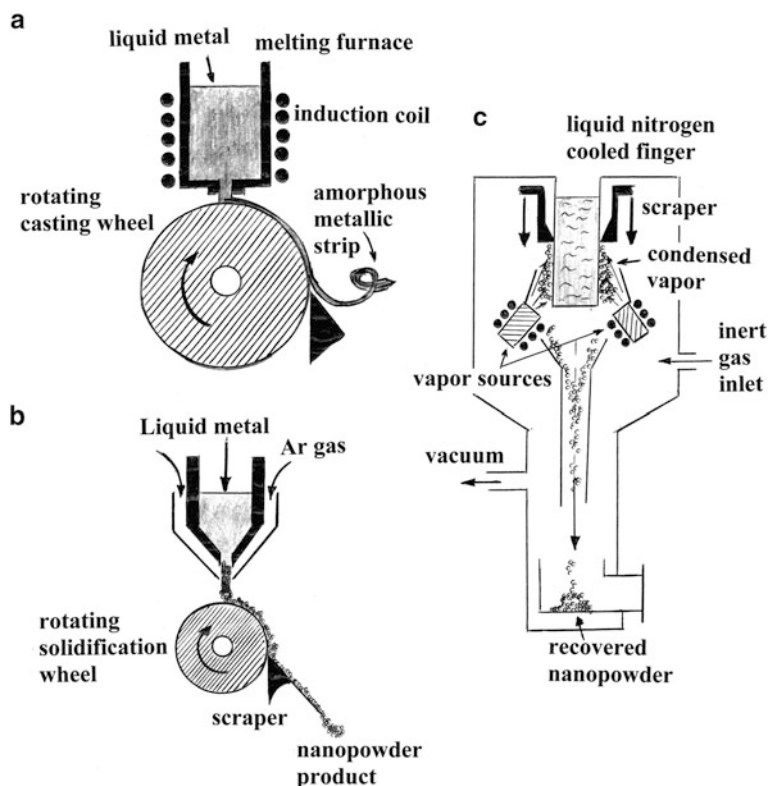


**Fig. 3** Supercooling/rapid solidification processes. (a) Supercooled rotating casting drum process for producing amorphous metal or alloy ribbon. (b) Supercooled rotating drum process for producing nanoparticle product. (c) Evaporation–condensation process for nanoparticle (nanocrystalline) product synthesis. Evaporation sources are shown at S. Thermal evaporation is the most common source process

Figure 3c illustrates a later modification where vaporized metals or alloys were collected onto an extended cold finger or liquid nitrogen cooled cylinder fitted with a scraper assembly to systematically scrape the condensed, nanometal, or alloy product into a collection funnel, all in vacuum or an inert gas. This collection system in some cases also employed an assembly for consolidation of the powder using a piston and anvil assembly (Tjong and Chen 2004). Consolidated powder forms can then be placed in high-pressure piston–anvil assemblies to create nearly full density precursor billets for bulk nanomaterial fabrication.

Figure 4 compares common forms of physical vapor deposition (PVD) or chemical vapor deposition (CVD). As implicit in the designations, PVD is a physical (evaporation) process, while CVD is a chemical (reaction) process. As shown in Fig. 4a, a high-voltage or high-electric-field condition can create a plasma in an inert gas environment which strips electrons from the gas atoms and creates positive ions with an energy related to the electric field intensity. These ions interact

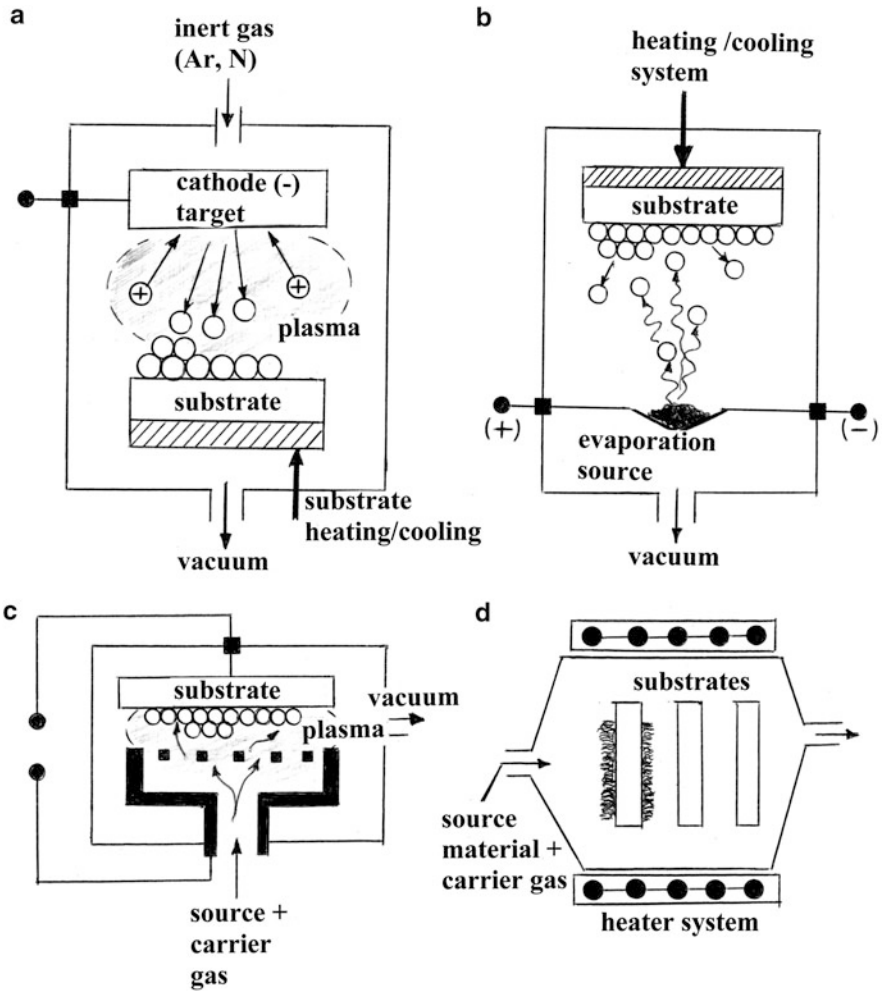


**Fig. 4** Comparison of common physical vapor deposition (PVD) and chemical vapor deposition (CVD) process schematics. (a) Ion sputtering onto heated or cooled substrate. (b) Thermal evaporation and condensation of vapor on heated or cooled substrate. (c) Plasma CVD process where reaction product is deposited onto a substrate. (d) Thermal CVD process having multiple substrates

with (or impact) the cathode target where the target atoms are sputtered from the surface and directed toward the substrate where they condense, forming discontinuous islands or continuous thin films, depending upon the sputter energy, sputter time, and substrate temperature. Lower substrate temperatures favor nanostructures, while higher temperatures favor larger, continuous grain structures or even single-crystal films which can be nanometers in thickness. The structure of

the substrate (crystalline or noncrystalline) can also influence the sputter-deposited product.

Another more common form of PVD involves metal or alloy evaporation or even multiple source evaporation to create some required stoichiometry on the substrate surface. In this process, shown in the simple schematic of Fig. 4b, a material is evaporated from a source configuration using a number of forms of evaporative heating, the simplest of which is resistive heating in a “boat.” This process is accomplished in a vacuum, often a very high ( $10^{-5}$  Torr) or ultrahigh ( $>10^{-9}$  Torr) vacuum. The evaporating atoms are deposited on a substrate, either crystalline or noncrystalline, which may be heated or cooled. These parameters, along with the rate of evaporation, can be used to control the structure and continuity of the deposit. Deposits can become single-crystal films in contrast to nearly amorphous or nanograin films. The deposition process itself can involve a number of phenomena: adsorption, desorption, deposition, diffusion, nucleation, and growth. These will be treated briefly in Fig. 7b following.

In CVD processes, precursor components or some materials and a carrier gas, which can include water vapor, are mixed or injected into a plasma plume and reacted to form a prescribed nanomaterial which deposits on a substrate. Alternatively, the reaction proceeds in a thermal environment where the reaction product is deposited on a substrate or multiple substrates. These two processes are illustrated in Fig. 4c, d, respectively. It is apparent that the plasma CVD process in Fig. 7c is conceptually very similar to the plasma deposition processes of Fig. 1b. CVD processes (Fig. 4c, d) allow both thin films and nanoparticulates (nanopowders) to be fabricated, often in multiple substrate arrays as shown schematically in Fig. 4d. In most conventional CVD processing thin films form on the substrate, but process parameter adjustments can allow nanoparticle deposits instead of films. This form of deposition is also called *chemical vapor synthesis* (CVS). Precursor materials can be metalorganics (where the process is referred to as metalorganic CVD or MOCVD), carbonyls, hydrides, chlorides, or other volatile compounds in gaseous-, liquid-, or solid-state forms. Reactions, as illustrated, can be laser-assisted, microwave, or RF plasma processes.

CVD processes using hydrocarbon and especially hydrocarbon gas precursors are used to produce carbon nanotubes and diamond films as well as graphene, usually in high-temperature reactors or the so-called tungsten hot-wire reactors illustrated schematically in Fig. 5. Figure 5a employs metal nanoparticle catalysts either on substrate arrays or in some nanoparticle spray form which nucleates multiwall carbon nanotubes (MWCNTs). Simple mechanisms for this process are illustrated schematically in Fig. 5b, while Fig. 6b shows metal-catalyst-formed MWCNTs in comparison with graphite (or carbon) *arc-evaporation-produced* MWCNTs in Fig. 6a. In Fig. 5c, methane and hydrogen are injected into the system where the  $H_2$  striking the hot W wire breaks up into atomic hydrogen, H (or 2H), which decomposes the  $CH_4$  on the substrate surface forming either  $sp^3$  carbon (diamond) or  $sp^2$  graphite (graphene) hybridization, respectively, and hydrogen gas, depending on the CVD parameters. Graphene is usually deposited onto Cu, Ni, or Si



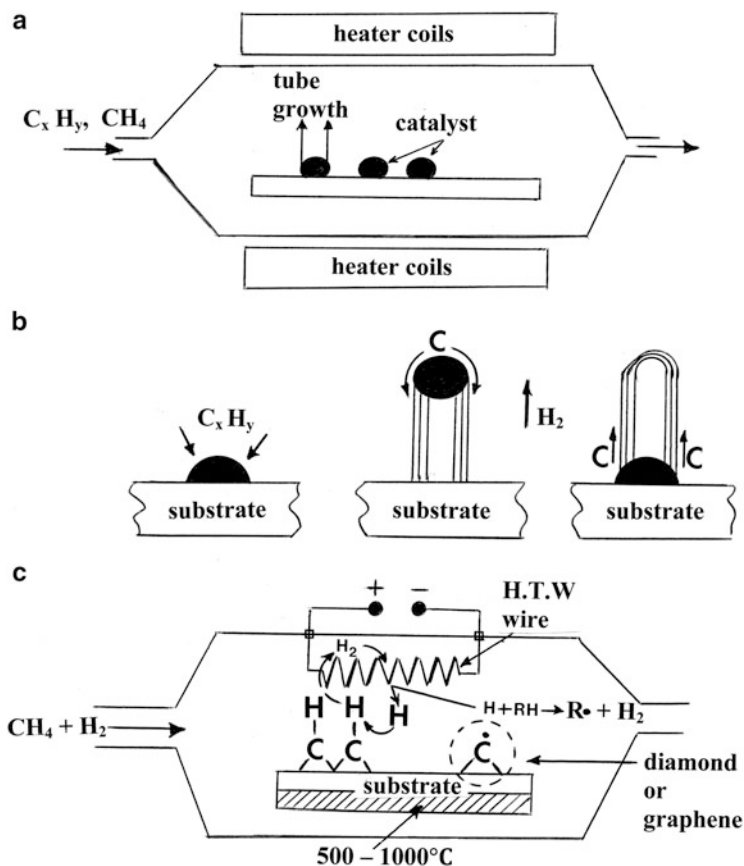
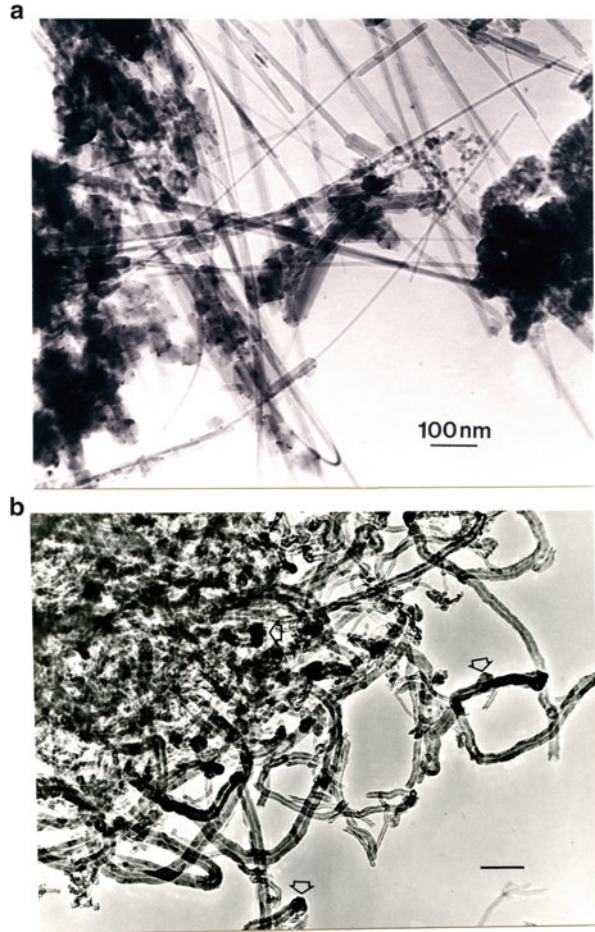


**Fig. 5** CVD metal-catalyst-assisted growth of carbon filaments and multiwall carbon nanotubes (MWCNTs) from hydrocarbon precursors,  $C_x H_y$  ((a) and (b)). (b) Shows tip growth and base growth mechanisms for MWCNTs on metal catalyst nanoparticles. Adapted from Kumar and Ando (2010). (c) Growth of diamond films or graphene on heated substrate from methane precursor using a tungsten hot-wire process

substrates where it can be washed away and transferred to another desired substance surface.

In some cases, it is important to be able to fabricate multilayer nanocomposites, especially semiconductor heterojunction or related structures by the systematic deposition of nanolayers forming single-crystal films. This process is usually described in some form of *molecular beam epitaxy* (MBE), atomic layer epitaxy (ALE), or atomic layer deposition (ALD) as illustrated schematically in Fig. 7a. In this ultrahigh vacuum process, separate evaporation or effusion cells form a gaseous (vapor) element which is slowly deposited onto a single-crystal substrate. Often, co-deposition or multiple-element deposition of different elements occurs where these elements in predetermined stoichiometries react and grow epitaxially.

**Fig. 6** Comparison of multiwall carbon nanotube production by carbon arc evaporation (**a**) and CVD catalysis (**b**). Arrows show metal (Ni) nanoparticles at tube ends. (**a**) and (**b**) are TEM images



For example, Al, Ga, and As can form predetermined layers of Al Ga As or Al As on Ga As and alternating in specifically defined nanothickness layers. Epitaxy occurs when the growing layers or films assume the crystal structure of the substrate. If the growth layer and substrate do not match in terms of unit cell dimensions, a mismatch occurs which produces interfacial strain. Such strained-layer device structures or strained-layer superstructures can have unique microelectronic and optoelectronic properties which are described in Part XV. Such structures are often referred to as quantum well or strained multiple-quantum well structures. Figure 8 illustrates a high-resolution TEM image of alternating Ga As and Al As layers. These structures are also referred to as atomic layer structures or superlattice structures. In some cases, deposited layers perfectly match the substrate crystal structure even though their lattice parameters do not match. As noted, this causes a strained lattice, and the process is called *pseudomorphic growth*. At some thickness, these layers may revert to the unit cell

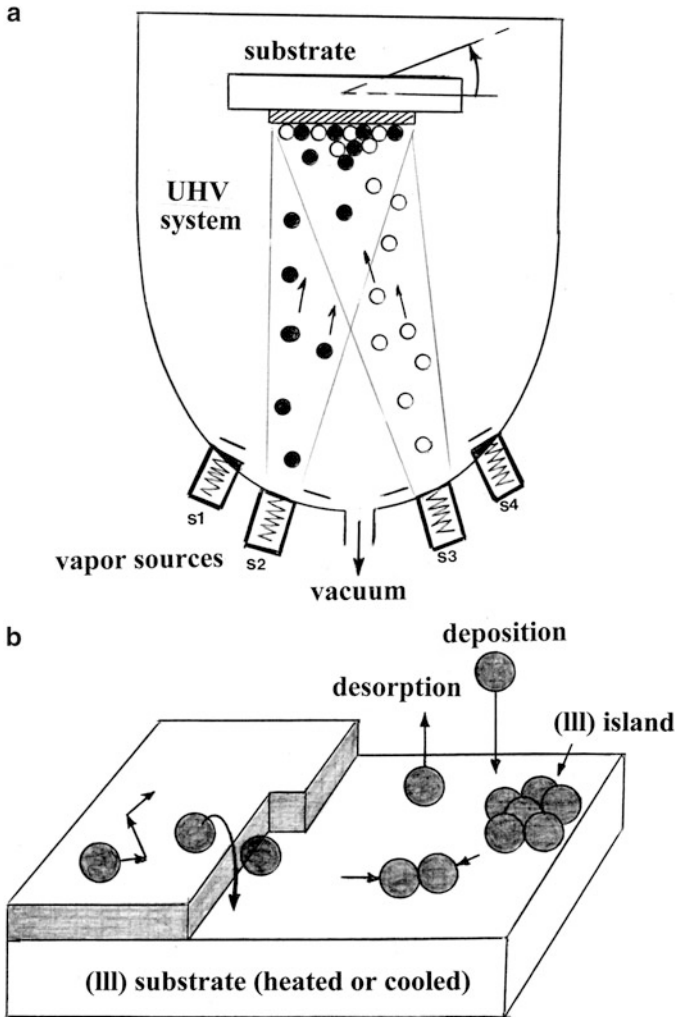


**Fig. 7** MBE process schematic (a). Effusion (vapor) sources are noted 1, 2, 3, 4. Each source has a shutter arrangement. The substrate can be tilted or translated as necessary. It can also be heated or cooled. (b) Shows a cartoon depicting the overall deposition process on a crystalline substrate. (111) layer growing on (111) substrate. Diffusion of atoms on the surface and across and along growing edges is shown

dimension for the structure but still maintaining the orientation of the substrate in *epitaxial growth*. This transition is accommodated by dislocations forming at the interface.

The MBE process shown schematically in Fig. 7a is employed in electronic component/device fabrication where selective masking is used to selectively create device structures. These features will be described in more detail in

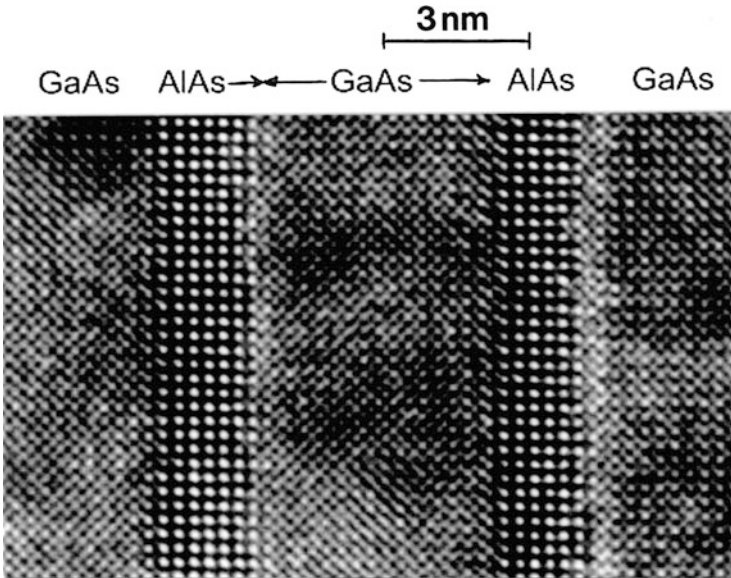


**Fig. 8** High-resolution TEM image of alternating GaAs and AlAs MBE-deposited layers in cross section (Courtesy of Simone Montanari, University of Liverpool)

Part XV. Masking can also be used to create periodic arrays of quantum dots and similar nanoparticle arrays on a substrate.

Figure 7b illustrates various phenomena involved in the deposition of atom species on a substrate and the growth of islands or thin films. In pseudomorphic or epitaxial growth, the island or film structure will be characteristic of the substrate crystal surface structure. Deposited atoms can, under some circumstance, desorb or leave the surface. For energetic (ballistic) atoms striking the surface, they may simply rebound. In some processes, this is characterized by a sticking coefficient or probability which is related to the fraction of atoms sticking or depositing. A probability of one implies all atoms will stick. Atoms on the surface can diffuse as indicated in Fig. 8. Different surface plane configurations such as edges or ledges are more conducive to atoms being accommodated in comparison to atoms which simply reside alone on the surface. This has to do with the energetics associated with unsatisfied bonds: ideally (1) for a single atom on the surface, (2) for an atom at a layer edge, and (3) for an atom at a ledge (or kink) in the layer. Nucleating atoms can cluster together and take advantage of this bonding energetics. In contrast to PVD processes or CVD processes, MBE reaction occurs at the substrate or in the vicinity of the substrate and not in the vapor stream. In effect, the substrate catalyzes the reaction, and correspondingly the surface orientation influences the energetics associated with such catalysis in the same way it does where catalysts are applied, especially nanoparticle catalysts exposing different surface facets or crystal orientations. In the case of catalysis, the rate of

reaction is significantly influenced. Or the propensity of adsorption of a species is influenced.

Considering the crude model of Cao (2004), the surface energy associated with a crystal orientation will be given generally by

$$\gamma = N_b \epsilon_b \rho_a / 2 \quad (1)$$

where  $N_b$  is the number of broken bonds,  $\epsilon_b$  is the bond strength, and  $\rho_a$  is the surface atomic density or number of surface atoms per unit area on a newly created surface. For an fcc metal, for example, each surface atom on {100} facets would have four broken chemical bonds and Eq. 1 would become

$$\gamma(100) = 4\epsilon_b/a^2 \quad (2)$$

where  $a$  is the lattice parameter for the fcc unit cell. Similarly, {110} and {111} facets would have five and three broken bonds, respectively:

$$\gamma(110) = 5\epsilon_b/\sqrt{2}a^2 \cong 3.54\epsilon_b/a^2, \quad (3)$$

$$\gamma(111) = 2\sqrt{3}\epsilon_b/a^2 \cong 3.46\epsilon_b/a^2, \quad (4)$$

consequently  $\gamma(110) > \gamma(100)$ . Nanocrystals with high surface energy have an open surface structure and a high density of low-coordinated step and kink atoms (Fig. 7b). Such features usually lead to exceptional catalytic properties. However, fundamental thermodynamics (the second law) forms lower-energy surfaces (or facets composing nanocrystals) (Zhou et al. 2011).

Catalysts reduce the activation energy barrier for reactions, and surface structure and energy make a major contribution to lowering this energy. However, the mechanisms involved in such reactions and product deposition on crystal surfaces is complex since deposition on a surface alters the structure and corresponding surface energy. In addition, islands formed create edges, ledges, and corner structures (Fig. 7b) all with increasing energy associated with them. Figure 9 illustrates crystal structure facets typical of nanocrystalline particles and catalyst particles and the fundamental deposition cluster appearance on (100) and (111) facet orientations. Figure 10 shows a ball model view of what might be considered an epitaxial (100) quantum dot or related single-crystal nanoparticle nucleating in the (100) orientation, characteristic of the 4-atom nucleus on (100) in Fig. 9 (see Scott et al. 2003).

---

## Electrodeposition

Nanocrystalline deposits can be formed on a cathodic substrate in an ionic (DC) transport solution through a simple reaction of the form

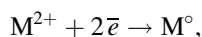
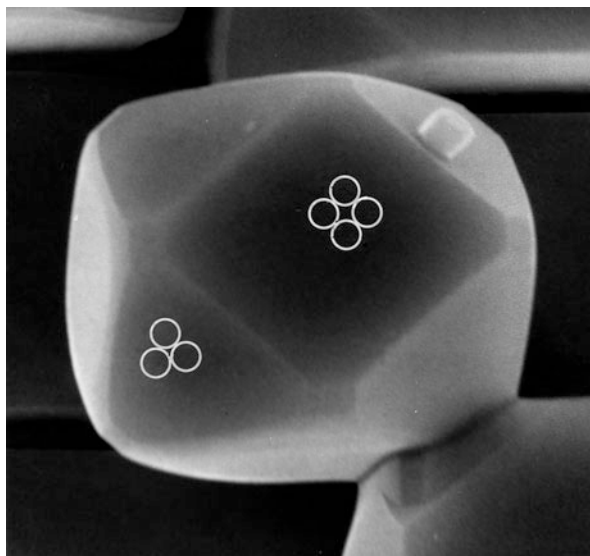


**Fig. 9** Faceted MgO (NaCl crystal structure) nanocrystal observed in the SEM. Primary cuboctahedron with small (110) facets at the (100) plane corners. Corresponding unit clusters on (111) and (100) plane facets are shown



**a**



**b**



**Fig. 10** [100] oriented ball model fcc crystal facet nanoparticle. **(a)** View down [100] axis. **(b)** Side view of nanoparticle model. Particle diameter is  $\sim 13$  atom diameters or  $\sim 25$  nm. True quantum dots would be roughly one fifth of this size or smaller. Note correspondence of (100) and {111} planes in **(a)** with Fig. 9

where M is a metal. The nanocrystal size and often nanostructure can be controlled by adjustment of bath composition, temperature, PH, current/voltage conditions, etc. Very fine grain or nanograin structure of electrodeposited coatings is often assured by using electrical pulses (*pulse plating*) where the pulse shape (current/voltage and time) can contribute to controlling the deposition parameters.

Notable examples of pulse plating have involved Ni (Robertson et al. 1999) and Cu (Lu et al. 2004). In the case of Ni, an equiaxed grain size of  $\sim 10$  nm could be achieved where the ultimate tensile strength (UTS) was measured to be  $>2$  GPa in contrast to  $10\ \mu\text{m}$  diameter grain size Ni electrodeposits where the UTS was 0.4 GPa. The corresponding Vickers microindentation hardness was 6.5 and 1.4 GPa, respectively (Robertson et al. 1999). Similarly, for electrodeposited nanocopper with a grain size of  $\sim 30$  nm, the UTS was measured to be  $\sim 1$  GPa in contrast to  $100\ \mu\text{m}$  grain size copper where the UTS was  $\sim 0.2$  GPa (Lu et al. 2004). In either case, the difference in UTS or microindentation hardness was roughly a factor of 5. In the case of Cu, nanotwins (growth twins) also contributed to the microstructure development since the twin (or twin boundary) interfacial free energy is nearly half for Cu in contrast to Ni (see Part V, chapter “► Planar Defects: Crystal Interfaces”).

---

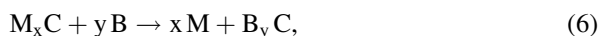
## Fabrication of Bulk Nanocrystalline Materials by Severe Plastic Deformation Processes

Nanoparticulate materials, even amorphous particulates fabricated as illustrated in Fig. 3, can be consolidated using a high-pressure (static) punch and anvil (or die) arrangement or by explosive (shock) consolidation which can apply very large dynamic pressure at relatively low temperatures ( $\leq 100^\circ\text{C}$ ) (Murr 1988). Consolidation of cylindrical forms which can be used as billets as precursors for extrusions or other forming processes can produce nearly fully dense material.

In related, severe (plastic) deformation processes, high strain and strain rate (including impact or ballistic conditions) can create grain refinement by *dynamic recrystallization* driven by localized, adiabatic strain heating generally expressed by

$$\Delta T \sim \epsilon \times \dot{\epsilon} \quad (5)$$

where  $\Delta T$  is the temperature gradient,  $\epsilon$  is the strain, and  $\dot{\epsilon}$  is the associated deformation strain rate. Such localized temperature gradients can drive chemical reactions in mixtures of oxides, chlorides, etc. These processes are often referred to as *mechanochemical synthesis* which can be characterized by the following displacement reaction:



where  $M_xC$  and B are precursor materials (M designating a metal). These materials or materials mixtures can be agglomerates which are placed in a ball mill or attriter

where repeated impacting can drive both a reaction as shown in Eq. 6 and grain or crystal refinement by dynamic recrystallization implicit in Eq. 5. This process can also be conducted where metal or alloy aggregates are not chemically reacted but are plastically deformed to create a dynamically recrystallized regime involving nanograins which can flow into one another and mix in the solid state. This process creates a *mechanical alloy* by repeated deformation in a ball mill or attrition, creating alloyed or immiscible mixtures and nanocrystalline aggregates (see Zehetbauer and Zhu 2009). The aggregates can form larger clumps which can be statically or dynamically consolidated as described above to create precursor billets for conventional processing: extrusion, forging, rolling, etc. Some of these features will be discussed in more detail in Part XIII which follows.

There are two other novel, extreme plastic deformation or *severe plastic deformation (SPD)* processes which can create nanocrystal or nanograin structures by dynamic recrystallization. These include friction-stir processing (FSP), a modification of friction-stir welding to be described in detail in Part XIII, and equal-channel angular processing (or pressing) (ECAP). In the former FSP concept, a rotating tool is translated along the surface, or within some depth of the surface, of a usually flat plate metal or alloy having a more conventional grain structure ( $\geq 100 \mu\text{m}$ ). This rotating tool causes the material to dynamically recrystallize and flow in the solid state. That is, the dynamically recrystallized grains (usually in the higher nanoregime:  $> 500 \text{ nm}$ ) will glide one over the other (grain boundary sliding). As illustrated in Fig. 11, this process can create a nanocrystalline layer on the surface of a conventionally processed plate, or a thin layer of some new material (metal or alloy) can be deposited on the surface of the plate, and then stir processed to create a nanocrystalline regime. This stir processing can be controlled by the length of the stirring tool as well as the rotation and translation speeds, which can alter the strain and strain rate as implicit in Eq. 5. The stir processing can raster across a selected surface area or process the entire surface, creating an engineered surface layer.

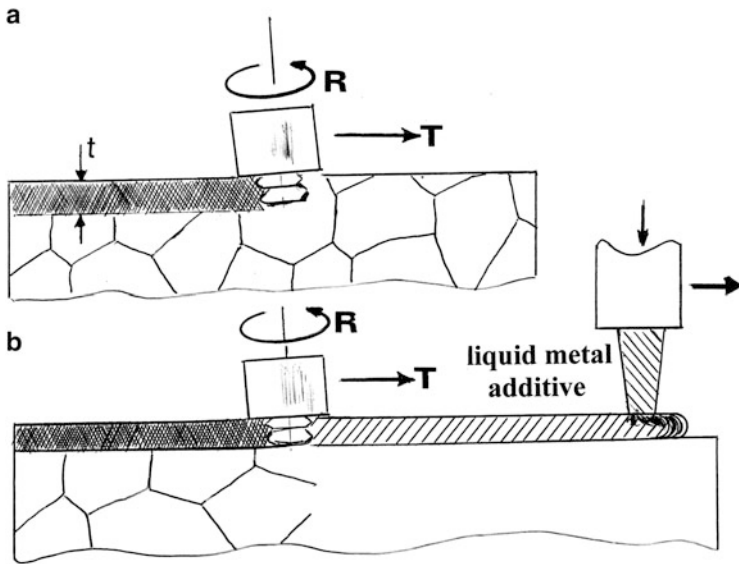
In the ECAP process (also referred to as *equal-channel angular extrusion*) illustrated schematically in Fig. 12, precursor powders or precursor consolidated billets can be further refined to produce very small nanocrystalline grain structures, or more conventionally processed metal or alloy billets having conventional grain sizes  $\sim 100 \mu\text{m}$  can be strained to create dynamic recrystallization producing nanocrystal grain structures.

Precursor billets are pressed through the die arrangement shown in Fig. 12 using a plunger. The die geometry, or angular relationships, governs the effective strain ( $\epsilon$ ) according to the relationship

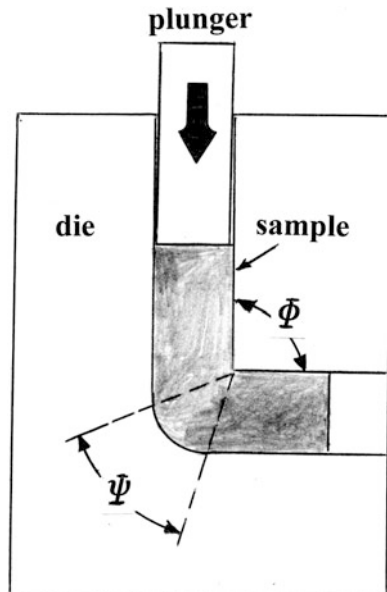
$$\epsilon = [2 \cot(\phi/2 + \varphi/2) + \varphi \operatorname{cosec}(\phi/2 + \varphi/2)]/\sqrt{3}. \quad (7)$$

Figure 13 illustrates effective stress contours for a finite element analysis in the recent work of Nagasekhar et al. (2007) as the inside die angle,  $\phi$ , was changed. Corresponding to larger effective stresses or strains in response to ECAP die angles implicit in Fig. 13 or Eq. 7, Figure 14 illustrates a few examples of the nanograin sizes achieved for different die angles (creating the effective strains noted as





**Fig. 11** Friction-stir processing of bulk plate surface (a) and additive surface layer (b). The additive layer can be laser-assisted direct metal deposition, laser-engineered net shape deposition, etc. See Part XI. R and T in (a) and (b) refer to the pin tool rotation (*R*) and traverse (*T*) speed. The tool is slightly off the normal axis as shown for efficient stir processing



**Fig. 12** Equal-channel angular processing (or pressing) (*ECAP*) for grain refinement

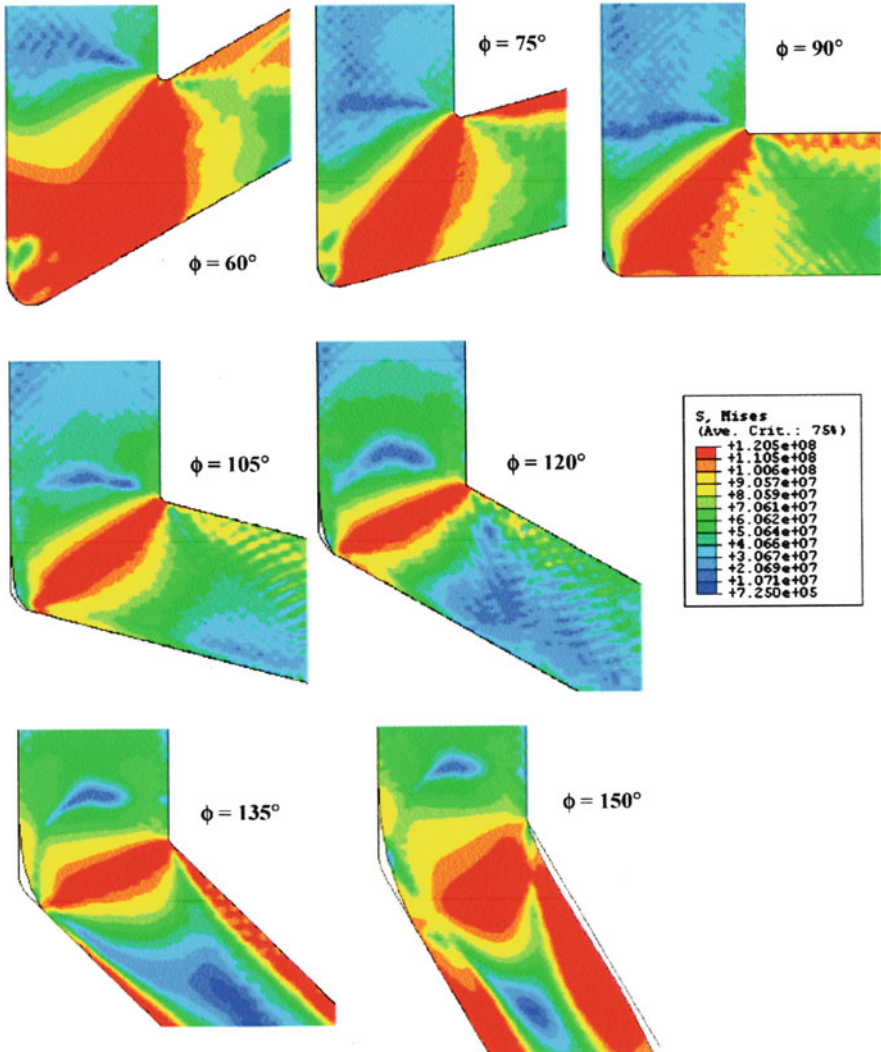


**Fig. 13** Finite element simulations for effective stress contours related to different ECAP channel angles (Adapted from Nagasekhar et al. (2007))

expressed in Eq. 7), with a single pass of the precursor billet, as well as multiple passes at a constant  $90^\circ$  die angle. Strain is partly cumulative, but in addition, grains can be restructured by repeated dynamic recrystallization which can result in grain texture as well as increasing grain boundary misorientation (higher energy grain boundaries). Variations of the so-called process routes in ECAP can produce elongated grains (texture) as well as equiaxed grains implicit in Fig. 14c (Valiev and Longdon 2006).

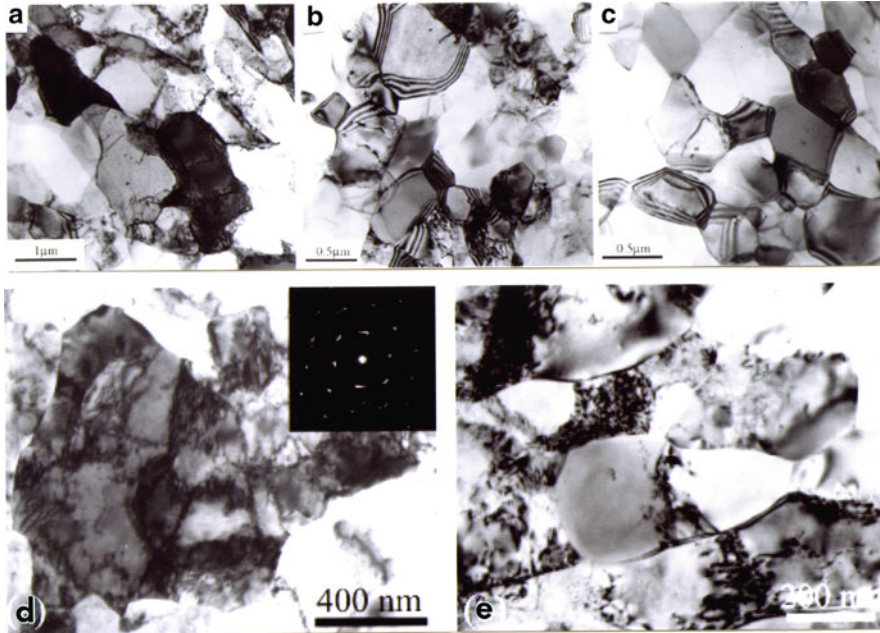


**Fig. 14** TEM image examples of nanograin structures related to ECAP processing. (a) to (c) are Al processed at equivalent strains of 2, 4, and 8, respectively. (d, e) show Cu processed at an angle  $\phi = 90^\circ$ ; 4 and 24 passes, respectively. SAED pattern insert in (d) shows some arcing of spots due to small grain size. (a–c) (Courtesy of A.A. Kibar, Middle East Technical University; (d, e) are courtesy of C.X. Huang, Shenyang National Laboratory for Materials Science, Shenyang, China)

Bulk nanometals such as those processed by ECAP can exhibit superplasticity because the nanograins promote easy grain boundary sliding rather than more conventional, dislocation-driven deformation. These properties and performance issues will be discussed later.

## References

- Ahmad P, Mukherjee S, Senapati D, Mandal MI, Khan RK, Sastry M (2003) Extra cellular biosynthesis of silver nanoparticles using the fungus *Fusarium oxysporum*. *Colloids Surf B Biointerfaces* 28:313–318
- Anastas PT, Warner JC (2000) *Green chemistry: theory and practice*. Oxford University Press, New York
- Brinker CJ, Scherer GW (1990) *Sol–gel science: the physics and chemistry of sol–gel processing*. Academic, New York
- Cao G (2004) *Nanostructures and nanomaterials: synthesis properties and applications*. Imperial college Press, London
- Das SK, Marsili E (2010) A green chemical approach for the synthesis of gold nanoparticles: Characterization and mechanistic aspect. *Rev Environ Sci Biotechnol*. Published online 4 Feb 2010. doi:10.1007/S11157-010-9188-5

- Kumar M, Ando Y (2010) Chemical vapor deposition of carbon nanotubes: a review on growth mechanisms and mass production. *J Nanosci Nanotechnol* 10:3739–3758
- Lu K (1996) Nanocrystalline metals crystallized from amorphous solids: nanocrystallization, structure and properties. *Mater Sci Eng R* 16:161–221
- Lu L, Shen Y, Chen X, Qian L, Lu K (2004) Ultrahigh strength and high electrical conductivity in copper. *Science* 304:422–426
- Marchiol L (2012) Synthesis of metal nanoparticles in living plants. *Ital J Agron* 7(e37):274–282
- Murr LE (ed) (1988) Shock waves for industrial applications. Noyes, Park Ridge
- Nagasekhar AV, Tick-Hon Y, Seow HP (2007) Deformation behavior and strain homogeneity in equal channel angular extrusion/pressing. *J Mater Process Technol* 192–193:449–452
- Robertson A, Erb U, Palumbo G (1999) Practical applications for electrodeposited nanocrystalline materials. *Nanostruct Mater* 12:1035–1040
- Scott SL, Crudden CM, Jones CW (eds) (2003) Nanostructured catalysts, Nanostructure science and technology series. Springer, New York
- Tjong SC, Chen H (2004) Nanocrystalline materials and coatings. *Mater Sci Eng R* 45:1–88
- Valiev RZ, Longdon TG (2006) Principles of equal-channel angular pressing as a processing tool for grain refinement. *Progress in Materials Science*, vol 51. Issue 7, Elsevier, New York
- Zehetbauer MJ, Zhu YT (eds) (2009) Bulk nanostructured materials. Wiley-VCH, Weinheim
- Zhao P, Li N, Astroe D (2013) State of the art in gold nanoparticle synthesis. *Coord Chem Rev* 257:638–665
- Zhou Z-Y, Tian N, Li J-T, Broadwell I, Sun S-G (2011) Nanomaterials of high surface energy with exceptional properties in catalysis and energy storage. *Chem Soc Rev* 40:4167–4185